RSC Advances

ROYAL SOCIETY OF CHEMISTRY

www.rsc.org/advances

RSC Advances

RSCPublishing

ARTICLE

Impact of postdeposition annealing on the sensing and impedance characteristics of TbY_xO_y electrolyte-insulator-semiconductor pH sensors

Cite this: DOI: 10.1039/x0xx00000x

Received 2 May 2016,
Accepted XXth XXX 2016

DOI: 10.1039/x0xx00000x

www.rsc.org/

Tung-Ming Pan,*[a,b] Ching-Yi Chen[a], Tung-Yu Wu,[a] and See-Tong Pang[b]

In this paper, we explore the impact of postdeposition annealing (PDA) on the sensing and impedance characteristics of TbY_xO_y sensing films deposited on Si(100) substrates through reactive cosputtering for electrolyte-insulator-semiconductor (EIS) pH sensors. The TbY_xO_y EIS sensor annealed at the 800 °C exhibited the best sensing characteristics (pH sensitivity, hysteresis voltage, and drift rate). In addition, the effect of PDA treatment on the impedance properties of TbY_xO_y EIS sensors was studied using the capacitance–voltage method. The resistance and capacitance of TbY_xO_y sensing films were determined using different frequency ranges in accumulation, depletion, and inversion regions. From the impedance spectroscopy analysis, the semicircle diameter of a TbY_xO_y EIS sensor becomes smaller due to a gradual decrease in the bulk resistance of the device with increasing the PDA temperature.

Introduction

An ion-selective field-effect transistor (ISFET) as a semiconductor device is currently constructed by replacing an ion-sensing membrane for the metal gate of a metal-oxide-semiconductor field-effect transistor (MOSFET).[1] The ISFET is able to respond to the surface potential change arising from the acid-base reactions occurring at the oxide-electrolyte interface. Semiconductor field-effect devices based on an electrolyte–insulator–semiconductor (EIS) system are generally the basic structural components of chemical and biological sensors. These devices have been established versatile tools for detecting pH, ion concentrations, enzymatic reactions, antigen-antibody recognition event, and DNA-hybridisation detection, etc.[2-4] The gate insulator material is an important element in an ISFET or EIS device, because no the metal gate electrode is directly in contact with the solution. The pH-sensitive ISFET or EIS devices, as the most widely used sensor, are fabricated with a large range of possible insulators (i.e. SiO_2, Si_3N_4, Al_2O_3, ZrO_2, and Ta_2O_5).[5-7] Although Si_3N_4 film is high strength, high thermal-shock resistance and good wear resistance, it is strongly reactive and can be readily oxidized upon exposure to air, thus leading to the degradation of sensing performance.[7-8] Apart from Si_3N_4 film, Al_2O_3 and ZrO_2 films as sensing materials are poor as a result of their low sensitivity and narrow pH range.[7] Nevertheless, Ta_2O_5 film has a higher sensitivity and lower drift compared with these materials,[7,9] but it deposited on the Si will produce a tantalum silicide layer and possessed a narrow band gap to degrade its electrical properties.[10] Consequently, it is not easy to achieve a reliable pH sensor with a high sensitivity and low drift.

The scaling of the gate dielectric has been made by shrinking the physical dimensions of complimentary metal-oxide-semiconductor (CMOS). A number of fundamental problems, e.g. high gate leakage current and oxide reliability, arise when the thickness of SiO_2 gate dielectrics approaches a limit (~2 nm). To overcome these fundamental limits, new high dielectric constant (κ) materials have been investigated.[11] Rare-earth (RE) oxide thin films, including La_2O_3, Nd_2O_3, Sm_2O_3, and Tb_2O_3,[12-14] have been widely investigated as alternative gate dielectrics for CMOS applications because they offer several advantages, including high dielectric constants, wide band gaps, large band offsets to Si, better thermal and thermodynamic stabilities. Among these RE oxides, terbium oxide (Tb_2O_3) has attracted recently a lot of attention as a promising high-κ gate dielectric due to its high conduction band offset, large band gap, and good thermal stability.[12,15] However, most high-κ RE oxide films are hygroscopic under air to produce a layer of hydroxide on their surface.[16] As a result, the surface roughness of RE oxides increases with the moisture absorption to deteriorate the electrical properties.[17] The problem can be solved by means of the incorporation of Ti or Y into the RE oxide film, hence resulting in less reactivity toward water.[16,18]

In an EIS structure, the charge and mass transfer at the interface of electrolyte and electrode have different time constants and can be modeled as a combination of resistors and capacitors. Generally, these consist of frequency independent resistive and capacitive components that indicate the charge

[a]*Department of Electronics Engineering, Chang Gung University, Taoyuan 333, Taiwan.*
[b]*Division of Urology, Chang Gung Memorial Hospital, Taiyuan 333, Taiwan.*
**Corresponding author: Dr. Tung-Ming Pan ;Fax: +886-3-2118507*
Tel: +886-3-2118800 Ext. 3349;E-mail: tmpan@mail.cgu.edu.tw

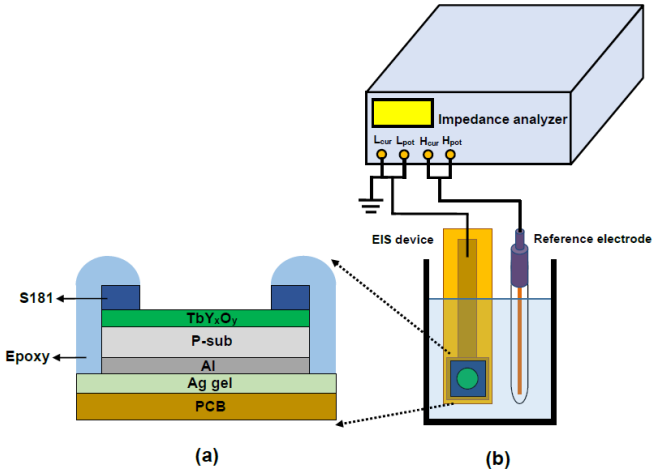

Fig. 1 Schematic illustration of (a) the structure of the TbY_xO_y EIS pH sensor and (b) the electrical measurement setup.

storage capacity and the relaxation times of individual process.[19-20] Impedance measurements as a function of frequency allow to realize the effects of interfacial layers helping evaluate the time constants related to the charge and mass transfer at the interface, or provide the information on capacitance/resistance changes occurring at conductive or semiconductive for sensing applications. Impedance spectroscopy is becoming an attractive electrochemical tool to characterize biomaterial films correspoding to electronic elements, thereby, allowing detection of biorecognition events at the surfaces. So far, to the best of our knowledge, experimental data associated with the impact of postdeposition annealing (PDA) on the impedance properties of the TbY_xO_y sensing films isn't studied. In this study, we described the sensing characterictics of the TbY_xO_y films deposited on a Si substrate by means of reactive co-sputtering and subsequent PDA at three temperatures. Furthermore, we investigated the impedance properties of the TbY_xO_y sensing films performed under accumulation, depletion and inversion regions, and measured in the pH 4, 7, 10.

Experimental

Fig. 1(a) demonstrates the EIS sensor structure with a TbY_xO_y sensing film. The TbY_xO_y EIS device was fabricated on a 4-in p-type (100) Si wafer. The Si substrates were cleaned by a standard RCA process and then by a diluted HF to remove the native oxide from the surface of Si wafer. Thin TbY_xO_y (~40 nm) films were deposited on the Si substrate through reactive co-sputtering from both Tb and Y targets in diluted O_2. Then, the PDA treatment of the films was carried out in a rapid thermal annealing (RTA) system with three annealing temperatures (700, 800 and 900 °C) under an O_2 ambient for 30 s. The backside contact (a 400-nm-thick Al film) of the Si wafer was deposited using a thermal coater. The sensing area of the deposited TbY_xO_y films was defined by an automatic robot dispenser with an adhesive silicone gel (S181) acted as an isolating layer. Finally, the EIS device was assembled on the copper lines of a custom-made printed circuit board by silver gel, and another adhesive epoxy was used to prevent leakage from the electrolyte.

The pH sensing performance of the EIS sensors was determined using standard buffer solutions in the pH range from 2 to 12. The capacitance–voltage (C–V) curves for the TbY_xO_y EIS sensors in the standard buffer solutions at different values of pH were then measured using a commercial Ag/AgCl reference electrode using a Hewlett–Packard (HP) 4284A LCR meter. Fig. 1(b) depicts that high potential

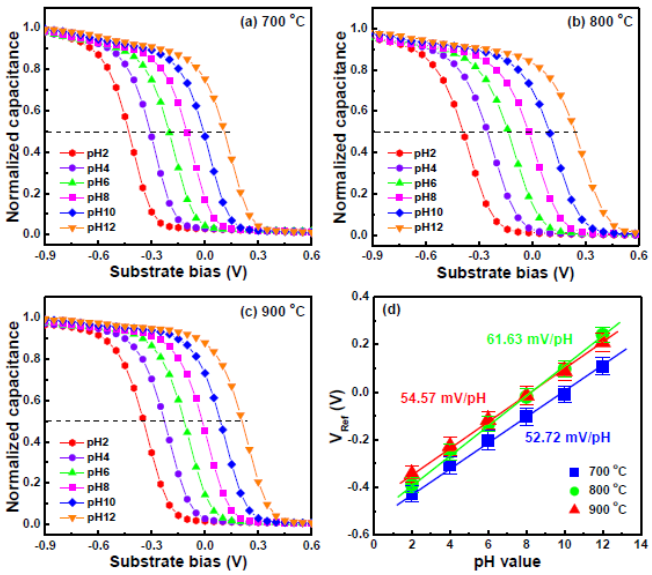

Fig. 2 (a) C–V curve responses for TbY_xO_y EIS devices annealed at (a) 700, (b) 800, and (c) 900 °C, when inserted into solutions at different pH values. (d) Reference voltage plotted as a function of pH for TbY_xO_y EIS devices annealed at three temperatures and measured at room temperature.

(H_{pot})/high current (H_{cur}) were applied to the electrode of Ag/AgCl reference and low potential (L_{pot})/low current (L_{cur}) to the electrode of an EIS device in the 4284A LCR meter. The GPIB address of the 4284A LCR meter was extracted onto the interface program, and then the computer started talking and listening to the 4284A LCR meter. The impedance measurement of EIS devices was performed using a combination of both HP 4284A (100 Hz – 500 kHz) and 4285A (500 kHz – 10 MHz) precision LCR meters in the frequency range from 100 Hz to 10 MHz. We used three sensors to measure their electrical properties. For a given experiment, each condition was tested in triplicate. To reduce any interference, all experimental setups were maintained in the dark and performed at room temperature.

Results and Discussion

A. Sensing characteristics of TbY_xO_y EIS devices

In an ISFET or EIS device, the flatband voltage (V_{FB}) is defined as:[21]

$$V_{FB} = E_{Ref} - \phi_0 + \chi_{sol} - \frac{\Phi_S}{q} - \frac{Q_{ox} + Q_{SS}}{C_{ox}} \quad (1)$$

where E_{Ref} is the potential of the reference electrode, ϕ_0 is the pH-dependent surface potential, χ_{sol} is the surface dipole potential of the solution, Φ_S is the work function of electrons in the semiconductor, q is the elementary charge, Q_{ox} and Q_{SS} are charges located in the oxide and the surface as well as interface states, respectively, and C_{ox} is the gate oxide capacitance. The flatband voltage was shifted by the surface potential, suggesting mainly dependent on the charge concentration. The site binding model was used to describe the proton transfer reactions at the oxide/solution interface. The oxide surface assumes the number of hydroxyl groups that can be found in a neutral state MOH, a positively charged (protonated) state MOH_2^+, or a negatively charged (deprotonated) state MO^-. The transduction of pH to a potential difference ϕ_0 between surface and bulk solution is performed through a pH dependent proton or hydroxide density

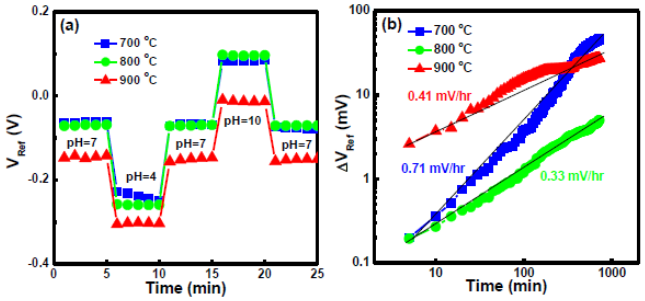

Fig. 3 Hysteresis characteristics as a function of time for TbY_xO_y EIS devices annealed at three temperatures, during the loop of pH 7→4→7→10→7. (b) Drift phenomena as a function of time for TbY_xO_y EIS devices annealed at three temperatures, tested at pH 7.

gradient. Under acid conditions, a Boltzmann-Poisson equation relates the surface potential to proton density difference:[22]

$$[H^+]_s = [H^+]_B \exp(-\frac{q\phi_0}{k_B T}) \quad (2)$$

where $[H^+]_x$ is the proton concentration at the oxide surface or in the bulk of the solution, q is the electron charge, k_B is Boltzmann's constant, and T is the absolute temperature. At a high pH value (small proton concentration in solution), the equilibrium is shifted toward a deprotonated surface which is negatively charged. Therefore, the C-V curve was shifted to the right. The relationship of surface potential and solution pH can be interpreted using the combination of the site-binding model and Gouy-Chapman-Stern theory to characterize the interface properties of the buffer solution and gate dielectric. The pH sensitivity of the gate dielectric surface can be expressed as:[21]

$$\frac{d\phi_0}{dpH} = 2.303\alpha \frac{k_B T}{q} \quad (3)$$

where α is a sensitivity parameter (dimensionless) which changes between 0 and 1 depending on the proton concentration of the buffer solution and the intrinsic buffer capacitance of the gate dielectric. The gate dielectric surface has the maximum value of pH sensitivity (59.5 mV/pH, at room temperature) if the α value is approaching to unity.

In general, the pH sensitivity of an EIS device is determined by the change in the flatband voltage per pH variation in the buffer solution. Fig. 2(a)-(c) depict the C–V curves of the TbY_xO_y EIS sensors annealed at 700, 800 and 900 °C. In an EIS pH sensing, a change in pH leads to a reference voltage (V_{Ref}) shift of the C–V curves as a result of ionization of the surface OH groups by H^+ or OH^- ions,[22] and thereby varying the surface potential through dipole formation on the sensing film. The V_{Ref} values were here calculated from the achieving C–V curves at a normalized capacitance of 0.5. The capacitance was normalized by dividing it by the capacitance value at the substrate voltage of -1 V. The TbY_xO_y EIS pH sensor exhibited a linear response with increasing the pH from 2 to 12. To estimate the pH detection sensitivities of the $TbTi_xO_y$ sensing films that had been subjected to various PDA temperatures, we recorded their C–V curves and then calculated their sensing performances. Fig. 2(d) demonstrates that the TbY_xO_y EIS sensor after PDA at the 800 °C exhibited a larger pH sensitivity of 61.63±3.5 mV/pH than those at other temperatures (52.72±3.4 mV/pH for 700 °C and 54.57±3.6 mV/pH for 900 °C). This result could be attributed to the optimal PDA temperature producing a rougher surface (see supplementary information), thus causing a higher surface site density in the TbY_xO_y film.[23] Moreover, pH sensitivity of this

TABLE I. pH response parameters for all $TbTi_xO_y$ samples including pH sensitivity, hysteresis voltage, and drift rate

PDA temperature (°C)	pH sensitivity (mV/pH)	Hysteresis voltage (mV)	Drift rate (mV/h)
700	52.72±3.4	14±1.3	0.71±0.06
800	61.63±3.5	1±0.1	0.33±0.02
900	54.57±3.6	6±0.6	0.41±0.03

TABLE II. Comparison of sensing performance for EIS or ISFET sensors fabricated with a Al_2O_3, Ta_2O_5, ZrO_2, CeO_2, Gd_2O_3, Y_2O_3, Tb_2O_3, and TbY_xO_y sensing film.

Sensing film	pH sensitivity (mV/pH)	Hysteresis voltage (mV)	Drift rate (mV/h)
Al_2O_3 [27]	52-58	~1	0.3
Ta_2O_5 [28]	55-58	~1	< 0.5
ZrO_2 [29]	57.1	X	~5.9
CeO_2 [25]	58.76	5.97	0.96
Gd_2O_3[30]	53.1	x	5.4
Y_2O_3 [31]	54.5	4.8	2
Tb_2O_3 [32]	56.97	12	0.446
TbY_xO_y	61.63	1	0.33

annealing temperature was higher than the theoretical value of 59.5 mV/pH. The super-Nernstian pH response of a TbY_xO_y EIS sensor could be associated with the adsorption of specific molecules[24] because PDA at 800 °C under an O_2 atmosphere could fill in the oxygen vacancies and dangling bonds,[25] thus leading to increases in the dielectric constant and the compact-layer capacity to change in the surface charge of TbY_xO_y film. Furthermore, this behaviour can contribute to the mechanism of one transferred electron per 1.5 H^+ ion.[26] During high temperature annealing, a thicker silicate layer can form at the TbY_xO_y–Si substrate interface.[12] The stability of the TbY_xO_y EIS sensor annealed at 800 °C was observed every three days. After 90 days, the sensitivity of this sensor was 60.48±3.7 mV/pH. The sensitivity of TbY_xO_y EIS sensor was stable.

In addition to the sensitivity detection, hysteresis and drift effects are two other important factors determining the success of an EIS sensor. Fig. 3(a) shows the hysteresis effect of the TbY_xO_y EIS sensor devices after PDA at three temperatures, directly immersed in each pH standard solution for up to 1500 s in set cycle of pH 7→4→7→10→7. Here, the hysteresis voltage is determined by the difference between the initial and terminal reference voltages measured in above cycle. The TbY_xO_y EIS sensor annealed at the 800 °C had the lowest hysteresis voltage of 1±0.1 mV among these temperatures (14±1.3 mV for 700 °C and 6±0.6 mV for 900 °C), presumably suggesting a stoichiometric TbY_xO_y film to suppress the oxygen vacancies and chemical defects, causing a lower number of crystal defects. In contrast, the film annealed at 700 °C exhibited a higher hysteresis voltage than other PDA temperatures, suggesting a higher density of crystal defects in its sensing film. Furthermore, we also estimated the drift effect of an EIS sensor by measuring the variation in the reference voltage after submerging it in a

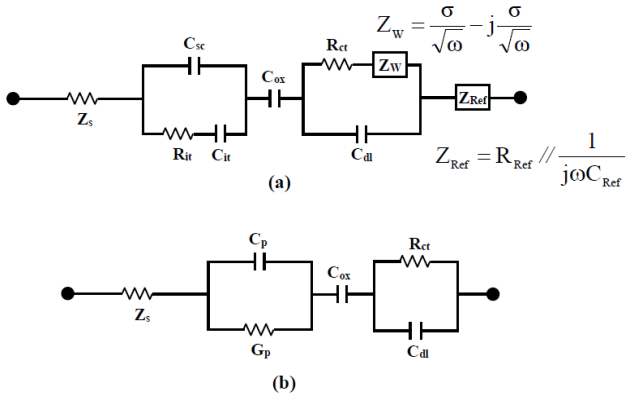

Fig. 4 (a) Model of circuit elements present when an EIS device is immersed in pH solution and (b) simplified equivalent circuit of an EIS device used in the study. Equivalent elements: Zs, Si substrate impedance; C_{sc}, space charge capacitance; C_{it}, interface trap capacitance; R_{it}, interface trap resistance; C_{ox}, gate oxide capacitance; C_{dl}, double-layer capacitance; R_{ct}, charge transfer resistance; Z_W, Warburg impedance; Z_{Ref}, reference impedance; C_p, frequency-dependent capacitance; G_p, frequency-dependent conductance.

standard buffer solution at pH 7 for up to 12 h. The change in the reference voltage can be defined as $\Delta V_{Ref}=V_{Ref}(t)–V_{Ref}(0)$. Fig. 3(b) depicts the drift characteristics of TbY_xO_y EIS sensors annealed at three temperatures. The slope of the reference voltage deviation stands for the stability of such an EIS sensor. The TbY_xO_y EIS device after PDA at 800 °C exhibited the best long-term stability (slope = 0.33±0.02 mV/h) than the other studied systems (0.71±0.06 mV/h for 700 °C and 0.41±0.03 mV/h for 700 °C), as shown in Table I. The lower drift rate might be attributed to the reduction in the oxygen vacancies and dangling bonds,[25] thus leading to lower ionic mobility. On the contrary, the sample annealed at 700 °C had a higher drift rate compared with other annealing temperatures, possibly suggesting a higher density of chemical defects in the film.

The measured and extracted sensing parameters are summarized in Table II, where the data from EIS or ISFET devices using a Al_2O_3,[27] Ta_2O_5,[28] ZrO_2,[29] CeO_2,[25] Gd_2O_3,[30] Y_2O_3,[31] and Tb_2O_3[32] sensing film, are shown for comparison. The TbY_xO_y sensing film has a better pH sensitivity than other sensing materials. The hysteresis voltage and the drift rate of TbY_xO_y sensing film are also comparable to those of Al_2O_3 and Ta_2O_5 films. Consequently, the TbY_xO_y sensing film is suitable for application to the EIS devices.

B. Impedance characteristics of TbY_xO_y EIS devices

Impedance spectroscopy is an effective method for probing the features of surface-modified electrodes.[33] A small amplitude perturbing sinusoidal voltage signal is applied to the electrochemical device, and the resulting current response is measured. The oxide–solution interface can be represented by an equivalent circuit, as shown in Fig. 4(a), where Z_S denotes the Si substrate impedance (parallel R_S and C_S circuit), C_{sc} the space charge capacitance, R_{it} and C_{it} the interface trap resistance and capacitance, respectively, C_{dl} the double layer capacitance, R_{ct} the charge (or electron) transfer resistance that exists if a redox probe is present in the electrolyte solution, Z_W the Warburg impedance arising from the diffusion of redox probe ions from the bulk electrolyte to the electrode interface, and Z_{Ref} the reference electrode impedance. Note that both Z_S and Z_W

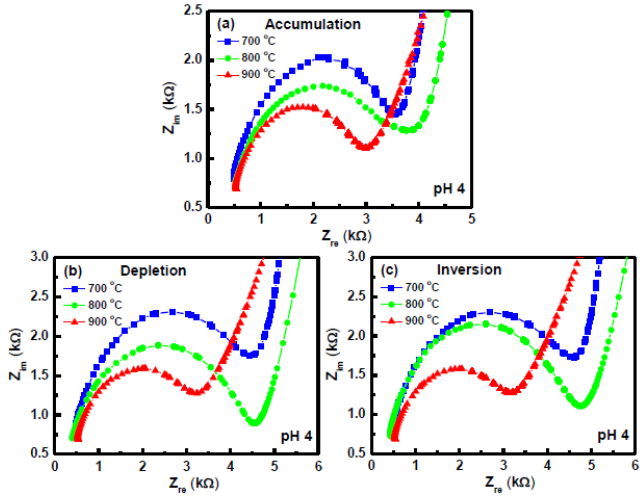

Fig. 5 Nyquist diagram (Z_{im} vs Z_{re}) of TbY_xO_y EIS devices annealed at three temperatures and performed in the (a) accumulation, (b) depletion and (c) inversion regions, immersed in pH 4.

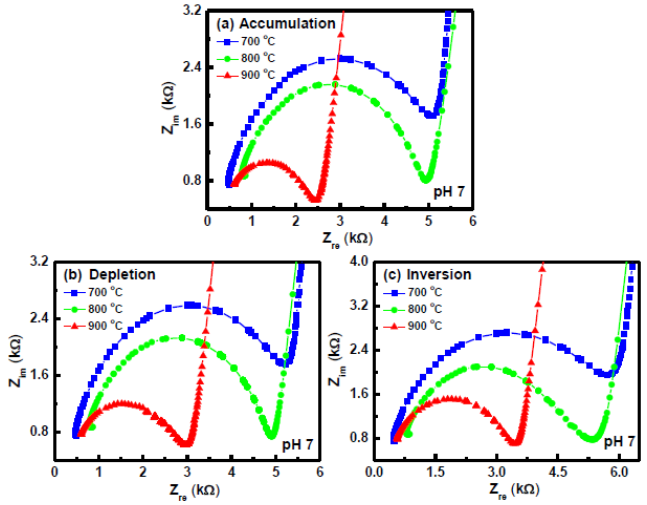

Fig. 6 Nyquist diagram (Z_{im} vs Z_{re}) of TbY_xO_y EIS devices annealed at three temperatures and performed in the (a) accumulation, (b) depletion and (c) inversion regions, immersed in pH 7.

represent bulk properties and are not expected to be affected by an EIS structure on an electrode surface. On the other hand, C_{dl} and R_{ct} depend on the dielectric and insulating properties of the oxide–electrolyte solution interface.

Figs. 5-7 show that Z_{Im} is plotted vs Z_{Re} as a function of frequency to obtain a Nyquist plot. A number of features can be identified in a Nyquist plot relying on the rate-determining processes at the oxide–solution interface. Figs. 5-7 depict a semicircle with a centre located on the Z_{Re} axis at higher frequencies, followed by a straight line at lower frequencies. The semicircle feature is usually related to the electron transfer-limited process, whereas the linear region is associated with the diffusion-limited process of the system. In addition, the semicircle is offset on the Z_{Re} axis (as $\omega \rightarrow \infty$) by a value corresponding to the magnitude of Z_S. For very rapid electron

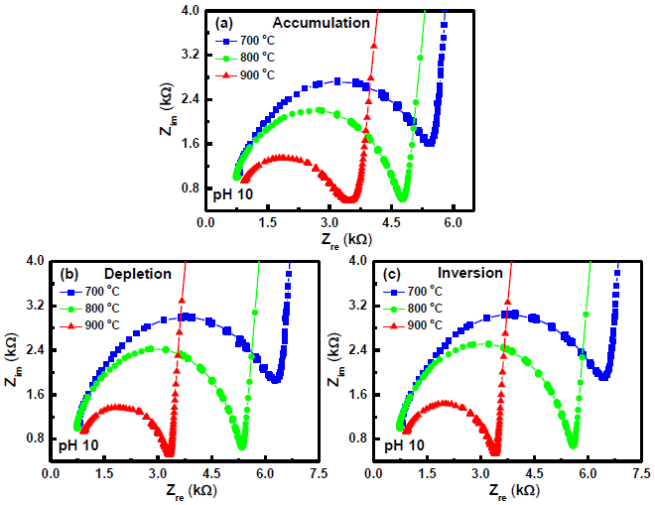

Fig. 7 Nyquist diagram (Z_{im} vs Z_{re}) of TbY_xO_y EIS devices annealed at three temperatures and performed in the (a) accumulation, (b) depletion and (c) inversion regions, immersed in pH 10.

transfer processes, the Nyquist plot will present the linear part of the impedance spectrum. In contrast, if the electron transfer process is the rate-determining step, the impedance spectrum will show a large semicircle without a straight line. Note that the diameter of the semicircle equals R_{ct} and extrapolation of the semicircle to lower frequencies will produce an intercept corresponding to (R_S+ R_{ct}). The MOSFET device under the depletion region, the conductance method is generally considered to be the most sensitive method to determine D_{it} in the depletion and weak portion of the band gap. It reflects the loss mechanism as a result of interface trap capture and emission of carriers.[34] If we consider the capacitance from the oxide and depletion to have small losses, then measured conductance under depletion stems from the contribution of the interfacial trap states. The simplified equivalent circuit of an EIS device appropriate for conductance method is shown in Fig. 4(b).

Based on the simplified equivalent circuit model in Fig. 4(b), two characteristic semicircles could be observed in the impedance plots: one is related to the bulk membrane response at higher frequencies, and another is associated with the oxide–solution interface response at lower frequencies. These TbY_xO_y EIS sensors show a single semicircle characteristic, as shown in Figs. 5-7. The frequency range of a single semicircle is from 0.1 to 10 MHz. Figs. 5(a)-(c) show that the radius of a semicircle for the film annealed at 700 °C was bigger than those at other temperatures, indicating the increase in bulk resistance of the EIS devices. In addition, the radius of the semicircle in the inversion region was larger compared with both accumulation and depletion regions.

In the pH 7, the impedance spectra of the TbY_xO_y EIS sensors annealed at three temperatures and performed under three regions were shown in Figs. 6(a)-(c). The diameter of the semicircle of an EIS device clearly decreased with increasing the PDA temperature. The diameter of a semicircle for an EIS device performed in the depletion region is higher than that of accumulation region. Nevertheless, the semicircle diameter of an EIS device measured in the inversion region becomes larger.

Figs. 7(a)-(c) depict the Nyquist plots of the impedance spectra of the TbY_xO_y EIS sensors annealed at three temperatures and measured at three regions. In the pH 10, the highest frequency leads to the lowest real impedance value (small semicircle), while the lowest frequency causes the highest real impedance value (large semicircle). The approximately semicircular plots in Figs. 5-7 are typically seen in simple electrochemical systems. The diameter of a semicircle in the pH 10 (alkaline solution) was bigger than that in the pH 4 (acid solution), suggesting a gradual increase in bulk resistance of the EIS devices with the pH value. The rate of diffusion of H_3O^+ ions was slower in comparison with the HO^- ions due to their larger size. Compared with both accumulation and depletion regions, the TbY_xO_y EIS device under the inversion region exhibited a higher impedance. Furthermore, the TbY_xO_y EIS device after PDA at 700 °C exhibited bulk resistance in the solutions with corresponding pH 4, 7, 10 that was higher than other PDA temperatures.

Conclusions

In this study, the impact of PDA on the sensing and impedance characteristics of TbY_xO_y sensing films deposited on Si(100) substrates through reactive cosputtering is explored. The TbY_xO_y EIS sensor after PDA at 800 °C exhibited a high pH sensitivity of 61.63 mV/pH, a small hysteresis voltage of 1 mV and a low drift rate of 0.33 mV/h. In addition, the impact of PDA on the impedance characteristics of TbY_xO_y EIS sensors was investigated by means of C–V method. The diameter of a semicircle for TbY_xO_y EIS device measured at the inversion region exhibited higher compared with both accumulation and depletion regions. Finally, the bulk resistance decreases upon increasing PDA temperature, whereas it increases with increasing pH value. The TbY_xO_y EIS sensor is suitable for use in electrochemical sensors and biosensors.

Acknowledgement

The authors thank the Chang Gung Memorial Hospital and the National Science Council of the Republic of China, Taiwan, for financially supporting this research under contracts of CMRPD2C0151, CMRPD2C0152, CMRPD2C0153, and NSC 102-2221-E-182-072-MY3.

References

1 P. Bergveld, *IEEE Trans. Biomed. Eng.*, 1970, **17**, 70.
2 P. Bergveld, *Sens. Actuators B*, 2003, **88**, 1.
3 A. Poghossian and M. J. Schoning, *Electroanalysis*, 2004, **16**, 1863.
4 M. J. Schoning and A. Poghossian, Analyst, 2002, **127**, 1137.
5 L. Bousse, H. H. van der Vlekkert, and N. F. de Rooij, *Sen. Actuators B*, 1990, **2**, 103.
6 D. Sobczynska and W. Torbicz, *Sens. Actuators*, 1984, **6**, 93.
7 D. H. Kwon, B. W. Cho, C. S. Kimo, and B. K. Sohn, *Sens. Actuators B*, 1996, **34**, 441.
8 S. M. Castanho, R. Moreno, and J. L. G. Fierro, *J. Mater. Sci.*, 1997, **32**, 157.
9 P. Gimmel, B. Gompf, and W. Gopel, *Sens. Actuators*, 1989, **17**, 195.
10 G. D. Wilk, R. M. Wallace, and J. M. Anthony, *J. Appl. Phys.*, 2001, **89**, 5243.
11 E. Gusev, *Defects in High-k Gate Dielectrics Stacks*, Springer, Dordrecht, 2006.
12 G. He and Z. Sun (Eds.), *High-k Gate Dielectrics for CMOS Technology*, Wiley-VCH Verlag GmbH & Co., Weinheim, 2012.
13 T. M. Pan, J. D. Lee and W. W. Yeh, *J. Appl. Phys.*, 2007, **101**, 024110.

14 T. M. Pan and C. C. Huang, *Electrochem. Solid-State Lett.*, 2008, **11**, G62.
15 S. Kitai, O. Maida, T. Kanashima, and M. Okuyama, *J. J. Appl. Phys.*, 2003, **42**, 247.
16 Y. Zhao, K. Kita, K. Kyuno, and A. Toriumi, *Appl. Phys. Lett.*, 2006, **89**, 252905.
17 Y. Zhao, M. Toyama, K. Kita, K. Kyuno, and A. Toriumi, *Appl. Phys. Lett.*, 2006, **88**, 072904.
18 T. Schroeder, G. Lupina, J. Dabrowski, A. Mane, Ch. Wenger, G. Lippert, and H. J. Mussig, *Appl. Phys. Lett.*, 2005, **87**, 022902.
19 A. J. Bard and L. R. Faulkner, *Electrochemical Methods*, Wiley India Edition, 2006.
20 C. A. Betty, R. Lal, and J. V. Yakhmi, *Electrochim. Acta*, 2009, **54**, 3781.
21 L. Bousse, N. F. De Rooij, and P. Bergveld, *IEEE Trans. Electron Devices*, 1983, **30**, 1263.
22 M. W. Shinwari, M. J. Deen, and D. Landheer, *Microelectron. Reliab.*, 2007, **47**, 2025.
23 C. S. Lai, C. M. Yang, and T. F. Lu, *Electrochem. Solid-State Lett.*, 2006, **9**, G90.
24 A. S. Poghossian, *Sen. Actuators B*, 1992, **7**, 367.
25 C. H. Kao, H. Chen, M. L. Lee, C. C. Liu, H. Y. Ueng, Y. C. Chu, C. B. Chen, and K. M. Chang, *Sen. Actuators B*, 2014, **194**, 503.
26 G. M. da Silva, S. G. Lemos, L. A. Pocrifka, P. D. Marreto, A. V. Rosario, and E. C. Pereira, *Anal. Chim. Acta*, 2008, 616, 36.
27 T. Matsuo, M. Esashi, and H. Abe, *IEEE Trans. Electron Devices*, 1979, **26**, 1856.
28 M. J.Schoning, D. Brinkmann , D. Rolka , C. Demuth, and A. Poghossian, *Sen. Actuators B*, 2005, **111-112**, 423.
29 K. M. Chang, C. T. Chang, K. Y. Chao and C. H. Lin, *sensors*, 2010, **10**, 4643.
30 L. B. Chang, H. H. Ko, M. J. Jeng, Y. L. Lee, C. S. Lai, and C. Y. Wang, *J. Electrochem. Soc.*, 2006, **153**, G330.
31 T. M. Pan and K. M. Liao, *Sen. Actuators B*, 2007, **128**, 245.
32 T. M. Pan, C. W. Wang, Y. S. Huang, W. H. Weng, and S. T. Pang, *J. Electrochem. Soc.*, 2015, **162**, B83.
33 E. Katz and I. Willner, *Electroanalysis*, 2003, **15**, 913.
34 E. H. Nicollian and J. R. Brews, *MOS (Metal Oxide Semiconductor) Physics and Technology*; Wiley: Hoboken, 2003.

